



Targeting IL-33 reprograms the tumor microenvironment and potentiates antitumor response to anti-PD-L1 immunotherapy

Yanyang Nan,¹ Yu Bai,¹ Xiaozhi Hu,¹ Kaicheng Zhou,¹ Tao Wu,¹ An Zhu,¹ Mengyang Li,¹ Zihan Dou,¹ Zhonglian Cao,¹ Xumeng Zhang,² Shuwen Xu,¹ Yuanzhen Zhang,¹ Jun Lin,¹ Xian Zeng,¹ Jiajun Fan,¹ Xuyao Zhang ¹, Xuebin Wang,³ Dianwen Ju ¹

To cite: Nan Y, Bai Y, Hu X, *et al.* Targeting IL-33 reprograms the tumor microenvironment and potentiates antitumor response to anti-PD-L1 immunotherapy. *Journal for ImmunoTherapy of Cancer* 2024;**12**:e009236. doi:10.1136/jitc-2024-009236

► Additional supplemental material is published online only. To view, please visit the journal online (<https://doi.org/10.1136/jitc-2024-009236>).

YN, YB, XH and KZ contributed equally.

Accepted 14 August 2024



© Author(s) (or their employer(s)) 2024. Re-use permitted under CC BY-NC. No commercial re-use. See rights and permissions. Published by BMJ.

For numbered affiliations see end of article.

Correspondence to

Dr Dianwen Ju;
dianwenju@fudan.edu.cn

Dr Xuebin Wang;
binxuewang@sjtu.edu.cn

Dr Xuyao Zhang;
xuyaozhang@fudan.edu.cn

ABSTRACT

Background The main challenge against patients with cancer to derive benefits from immune checkpoint inhibitors targeting PD-1/PD-L1 appears to be the immunosuppressive tumor microenvironment (TME), in which IL-33/ST2 signal fulfills critical functions. However, whether IL-33 limits the therapeutic efficacy of anti-PD-L1 remains uncertain.

Methods Molecular mechanisms of IL-33/ST2 signal on anti-PD-L1 treatment lewis lung carcinoma tumor model were assessed by RNA-seq, ELISA, WB and immunofluorescence (IF). A sST2-Fc fusion protein was constructed for targeting IL-33 and combined with anti-PD-L1 antibody for immunotherapy in colon and lung tumor models. On this basis, bifunctional fusion proteins were generated for PD-L1-targeted blocking of IL-33 in tumors. The underlying mechanisms of dual targeting of IL-33 and PD-L1 revealed by RNA-seq, scRNA-seq, FACS, IF and WB.

Results After anti-PD-L1 administration, tumor-infiltrating ST2⁺ regulatory T cells (Tregs) were elevated. Blocking IL-33/ST2 signal with sST2-Fc fusion protein potentiated antitumor efficacy of PD-L1 antibody by enhancing T cell responses in tumor models. Bifunctional fusion protein anti-PD-L1-sST2 exhibited enhanced antitumor efficacy compared with combination therapy, not only inhibited tumor progression and extended the survival, but also provided long-term protective antitumor immunity. Mechanistically, the superior antitumor activity of targeting IL-33 and PD-L1 originated from reducing immunosuppressive factors, such as Tregs and exhausted CD8⁺ T cells while increasing tumor-infiltrating cytotoxic T lymphocyte cells.

Conclusions In this study, we demonstrated that IL-33/ST2 was involved in the immunosuppression mechanism of PD-L1 antibody therapy, and blockade by sST2-Fc or anti-PD-L1-sST2 could remodel the inflammatory TME and induce potent antitumor effect, highlighting the potential therapeutic strategies for the tumor treatment by simultaneously targeting IL-33 and PD-L1.

INTRODUCTION

Immune checkpoint inhibitors (ICIs), especially those targeting programmed cell

WHAT IS ALREADY KNOWN ON THIS TOPIC

⇒ IL-33/ST2 signal pathway fulfills versatile roles in reprogramming immunosuppressive tumor microenvironment (TME), but whether this role is involved in immune checkpoint inhibitors therapy is uncertain.

WHAT THIS STUDY ADDS

⇒ This study identifies that the increased tumor-infiltrating ST2⁺ Treg cells as a critical risk factor for resistance to anti-PD-L1 treatment and provides novel strategies to augment the response of anti-PD-L1 monotherapy.

HOW THIS STUDY MIGHT AFFECT RESEARCH, PRACTICE OR POLICY

⇒ These findings suggested that blocking IL-33 could sensitize anti-PD-L1 therapy via promoting the formation of therapy-responsive TME, highlighting the potential clinical application.

death protein 1 (PD-1) and the PD-1 ligand (PD-L1), have been sanctioned for use in treating a diverse array of cancers. However, immunosuppressive tumor microenvironment (TME) hinders the response of patients with cancer to anti-PD-1/PD-L1 immunotherapy.¹⁻⁴ In TME, immunosuppressive cells and cytokines promote tumor development and play an essential role in resistance to PD-1/PD-L1 blockade.^{5,6} By targeting those immunosuppressive factors, the antitumor immune responses of PD-1/PD-L1 blockade can potentially be unleashed.^{7,8} Regulatory T cells (Tregs) with enhanced inhibitory ability are preferentially activated in anti-PD-L1 resistant solid tumors.¹ Although the depletion of Tregs using antibodies can partially reverse resistance to PD-1/PD-L1 ICIs, the non-specific depletion-inducing also leads to adverse effects^{7,9} and limits their application.

Similarly, the co-targeting of PD-L1 and TGF- β ,^{10–14} which reversed the increasing Treg/Th balance,^{15–16} showed modest antitumor activity in low immunogenicity tumor models.¹⁷ Consequently, there is a pressing need to clarify the immunosuppressive mechanisms and explore alternative strategies to boost the antitumor impact of PD-1/PD-L1 ICIs, particularly in immune-cold tumors.

Interleukin-33 (IL-33), belonging to the interleukin-1 (IL-1) superfamily, serves as a versatile cytokine that acts as an alarmin signal and is released in response to inflammation, biomechanical stress, or necrotic cell death.¹⁸ IL-33 is constitutively expressed in a range of cell types, such as epithelial cells, endothelial cells, and stromal fibroblasts.^{19–20} On interaction with its receptor, IL-33 forms a heterodimeric complex that comprises the suppression of tumorigenicity 2 (ST2) (also noted ST2L) and the IL-1 receptor accessory protein, triggering the activation of NF- κ B and MAPK pathways and leading to a range of subsequent responses in target cells.²¹ sST2, a soluble form of ST2, interferes with this interaction by binding with IL-33 as a decoy receptor. IL-33/ST2 axis plays a dual role in tumor progression.^{22–27} The specific role that IL-33 plays in tumor immunotherapy largely depends on several factors including cellular source, target cell type, and immunogenicity of TME.²⁸

It has been reported that IL-33/ST2 signal facilitated cancer progression and remodeled the TME by orchestrating the development and maintenance of immune suppressive cells.^{22–24–29} Tregs in TME featured with upregulated IL1RL1 (which encodes ST2) gene expression was preferentially proliferated and accelerated tumor progression on IL-33 treatment; conversely, genetic deficiency of IL1RL1 inhibited the expansion of Tregs in TME and delayed tumor growth.³⁰ Moreover, IL-33 specifically upregulated *Areg* expression in IL1RL1⁺ Tregs and developed an immunosuppressive state of cancer-associated fibroblasts (CAFs) via the AREG/EGFR axis, promoting tumor progression.³¹ In addition, IL-33 participates in the regulation of the immunosuppressive molecule TGF- β . After being released from tumor-initiating cells (TICs), IL-33 induced Fc ϵ RI α ⁺ macrophages differentiation with the secretion of TGF- β 1, which in turn signaled TICs to upregulate the release of IL-33 in TME.³² Nevertheless, it remains unexplored whether IL-33/ST2 signaling in modulating immunosuppressive TME limits the antineoplastic effect of PD-L1-targeting antibodies.

In this research, we explored the underlying cellular mechanism of IL-33/ST2 signal in the antitumor immunity of atezolizumab and the potential of IL-33 serving as a target to augment the efficacy of antitumor immune responses to anti-PD-L1 therapy. By using sST2-Fc to target IL-33, we examined the function of IL-33 during anti-PD-L1 therapy and explored the action mechanisms. More importantly, we developed bifunctional fusion proteins to simultaneously block the PD-L1 and IL-33 pathways and compared its antitumor activity relative to combination therapy, as well as unraveling its underlying

mechanisms, highlighting the potential therapeutic strategy for tumor immunotherapy by blocking IL-33 and PD-L1.

METHODS

Vector construction, protein expression, and purification

sST2-Fc: the cDNA encoding mouse ST2L (amino acids 27–332) was fused with the IgG1 domain of atezolizumab to construct the coding sequence of sST2-Fc. Anti-PD-L1 mAb: the cDNA encoding the light and heavy chains of atezolizumab. Heavy chain of bifunctional fusion proteins: fused the cDNA of sST2 via a flexible (Gly4Ser)₃Gly linker to the C-terminus of the heavy chain of atezolizumab for anti-PD-L1-sST2 or to the N-terminus for sST2-anti-PD-L1. Light chain of bifunctional fusion proteins: the cDNA encoding the light chain of atezolizumab. The complete sequence was cloned into the pTT5 plasmid vector after being digested by EcoRI and BamHI. All above proteins were expressed by transient transfection into 293-F cells and purified via a Protein A-Sepharose column.

Tumor model and treatments

Male wild-type BALB/c mice and C57BL/6 mice (20 \pm 2g body weight) were obtained from GemPharmatech (Nanjing, China) and raised under specific pathogen-free conditions. For subcutaneous tumor models, CT26 cells (5 \times 10⁵) and lewis lung carcinoma (LLC) cells (5 \times 10⁵) were inoculated on the right flank of mice, and therapy was initiated until the tumor tissue grew to 50–100mm³ (day 0). Tumor growth was monitored and estimated using the following formula: (long axis) \times (short axis)²/2. At time of sacrifice, tumor tissues were harvested, and the weight of each tumor was measured.

For metastasis models, CT26 cells (2 \times 10⁵) and LLC cells (2 \times 10⁵ or 5 \times 10⁵) were intravenously injected into the tail vein of mice on day –1 and treatment started at day 0. The survival status of metastasis CT26 model was monitored for 55 days. The lung metastasis LLC model (2 \times 10⁵) was monitored for 100 days after treatment, and the cured mice or untreated mice were rechallenged with 5 \times 10⁵ LLC cells and observed for further 3 weeks without treatment. Anti-PD-L1 (7.5 mg/kg) or equimolar proteins including sST2-Fc (6.3 mg/kg), and two forms of bifunctional fusion proteins (11.5 mg/kg) were intraperitoneally injected into the mice bearing subcutaneous or metastasis tumors on days 0, 4, 7, 11.

Flow cytometric analysis

For immune profiling of CT26 tumors in BALB/c mice, mice treatment with monotherapy or combination therapy at days 0, 4, 7. In LLC tumor model, the mice were given anti-PD-L1-sST2 or the above treatment at days 0, 4, 7, respectively. At day 10, tumor tissues of CT26 or LLC tumor model were harvested and prepared as single-cell suspensions for flow cytometry referring to a previous article.³³ According to the standard protocol, tumor single-cell suspensions were prepared and co-incubated

with the following reagents (all reagents purchased from Biolegend unless otherwise stated): anti-CD16/32 (101319), anti-CD45 (103116), anti-CD3 (100306, 100236), anti-CD4 (100406), anti-CD8 α (100707, 100723, 100729), anti-IFN- γ (505807), anti-Granzyme B (515408), anti-FOXP3 (126419), anti-CD44 (103012), anti-PD-1 (135216), anti-TIM-3 (119703), anti-TCF-1 (BD Biosciences, 566692) and FOXP3/Transcription Buffer (Invitrogen, 00-5523-00). Stained cells were analyzed by CytoFlex S (Beckman).

RNA-seq analysis

On the 10th day of treatment, tumor tissue RNA was extracted from the LLC tumor-bearing mice treated in the control group, monotherapy or combined therapy group ($n=3$) using Biozol RNA Miniprep Kit (BW-R7311, Peiwo). Subsequently, RNA libraries were prepared with the VVAHTS Universal V8 RNA-seq Library Prep Kit for Illumina (NR605-0, Vazyme) and sequenced on the Illumina NovaSeq 6000 platform. Shanghai Xu Ran Biotechnology Co. conducted mRNA enrichment, followed by fragmentation, reverse transcription, library construction, and executed the procedures for Illumina Novaseq 6000 sequencing.

StringTie (V.1.3.1c) was employed for generating gene expression data, and differential gene expression analysis was conducted using the DESeq2 package (V.1.16.1). Heatmap clustering of genes in the heatmap was achieved with WARD.D2, and normalization and visualization were performed using the Hiplot database (<https://hiplot.com.cn>). The volcano plot of differentially expressed genes (DEGs) ($\log_2FC=0.4$, $pCutoff=0.01$), excluding genes with 0 values, between the anti-PD-L1 and control groups was visualized using Rstudio.

Gene Ontology and KEGG enrichment analyses were carried out using the R package clusterProfiler, presenting the top 10 enrichments associated with immunity. Immune signature scores were calculated based on published lists13 and visualized with GraphPad Prism. Gene Set Enrichment Analysis (GSEA) was conducted using an online tool (<https://www.bioinformatics.com.cn>).

Single-cell RNA-seq (scRNA-seq)

LLC-tumor-bearing mice received 10 days of treatment with isotype control, atezolizumab, combined therapy, and anti-PD-L1-sST2 prior to tumor harvest. To ensure an adequate number of viable cells for sequencing postharvest, four tumors from each group were consolidated into a single sample due to the small size of the tumors. A total of 25,000 cells, with concentrations ranging from 700 to 1200 cells/ μ L, were loaded, and libraries were prepared following the guidelines of the 10X Genomics Next Chromium GEM Single Cell 3 Reagent Kits V.3.1 (Cat. 1000268). High-throughput sequencing took place on the Illumina Nova 6000 PE150 platform. The raw FASTQ files underwent processing using Cell Ranger software

(V.7.0.1), aligning them with the mm10 mouse reference genome.

scRNA-seq data analysis

Subsequent analyses were executed through the Seurat package (V.4.0.6) within the R package. Cells with fewer than 200 UMIs or more than 10% mitochondrion-derived UMI counts were identified as low-quality and excluded. The top 30 principal components, combined with the top 2000 variable genes, were employed in the analysis. The ScaleData function was used to regress out UMI count and the percentage of mitochondrion-derived UMI counts. Elimination of batch effects among distinct datasets was achieved using the R package harmony. Identification of main cell clusters occurred through the FindClusters function and set resolution equals 0.5 of Seurat, and visualization was achieved using two-dimensional uniform manifold approximation and projection, a widely recognized algorithm for data dimension reduction. Unsupervised clustering was applied for cell type discrimination, and markers for these cell types were identified through the analysis of differential gene expression, consistent with findings from prior studies.

Within the T cell population, the CD8_S1 cluster and CD8_S2 cluster exhibited high expression levels of Ccl5 and S100a4, signifying effector CD8⁺ T cells. The CD8_S3 cluster denoted tumor-infiltrating exhausted CD8⁺ T cells with elevated Pdcd1 and Lag3 expression. The CD4_S1 cluster displayed characteristics of effector CD4⁺ T cells, featuring Il7r gene expression. The Treg cluster showcased gene expression patterns of Foxp3 and Il2ra while the exhausted CD4_S2 cluster also manifested Mki67 and Top2a expression. Additional T cell clusters encompassed the PrCs cluster (marked by elevated expression of Cd8, Mki67, Top2a, Hmnr, Ezh2, and Cenpa), T-IFN cluster (exhibiting heightened expression of Rsad2 and Ifit3), NKT cluster (with increased expression of Cd8, Bcl2, Sell, and Klrb1c), and the CD4⁺CD8⁺ $\gamma\delta$ T cluster.³⁴

DEGs were identified through the utilization of the FindMarkers function. A significance threshold for DEGs was defined as $p<0.05$ and $|\log_2foldchange|>0.25$. Subsequent enrichment of GO and KEGG pathway analyses were carried out using R (V.4.0.3) based on the hypergeometric distribution. Gene set variation analysis (GSVA) used default sets from the molecular signature database, specifically GO: BP gene sets, as described in the GSVA package.

Statistical analysis

All data underwent statistical analysis using GraphPad Prism V.9.0, with results displayed as mean \pm SD or mean \pm SD. To determine the p value between groups, either Student's t-test or one-way analysis of variance was employed. * p or $^{\$}p<0.05$, ** p or $^{\$\$}p<0.01$ were considered to be significant statistical difference. For RNA-seq, data were processed in RStudio or online tools (hiplot.com.cn and www.bioinformatics.com.cn).

Other materials and methods are available in online supplemental file 1.

RESULTS

IL-33/ST2 interaction is implicated in the resistance to PD-1/PD-L1 blockade

To explore the relevance of IL-33/ST2 interaction to anti-PD-1/PD-L1 treatment resistance, the post-treatment expression levels of IL-33 and ST2 were assessed in tumors. In LLC mouse model, the RNA-sequencing

analysis unveiled a significant upregulation in *Il1rl1* gene expression (figure 1A,B). High expression of IL-33 and ST2 protein levels in tumor tissues during anti-PD-L1 treatment were exhibited, contrasting with no significant changes found in the serum (figure 1C–E and online supplemental figure 1). Meanwhile, IL-33/ST2 signals, such as MyD88, p-JAK2 and p-STAT3, were also upregulated after anti-PD-L1 injection (figure 1F and online supplemental figure 2). The results were further supported by immunofluorescence (IF), revealing a substantial

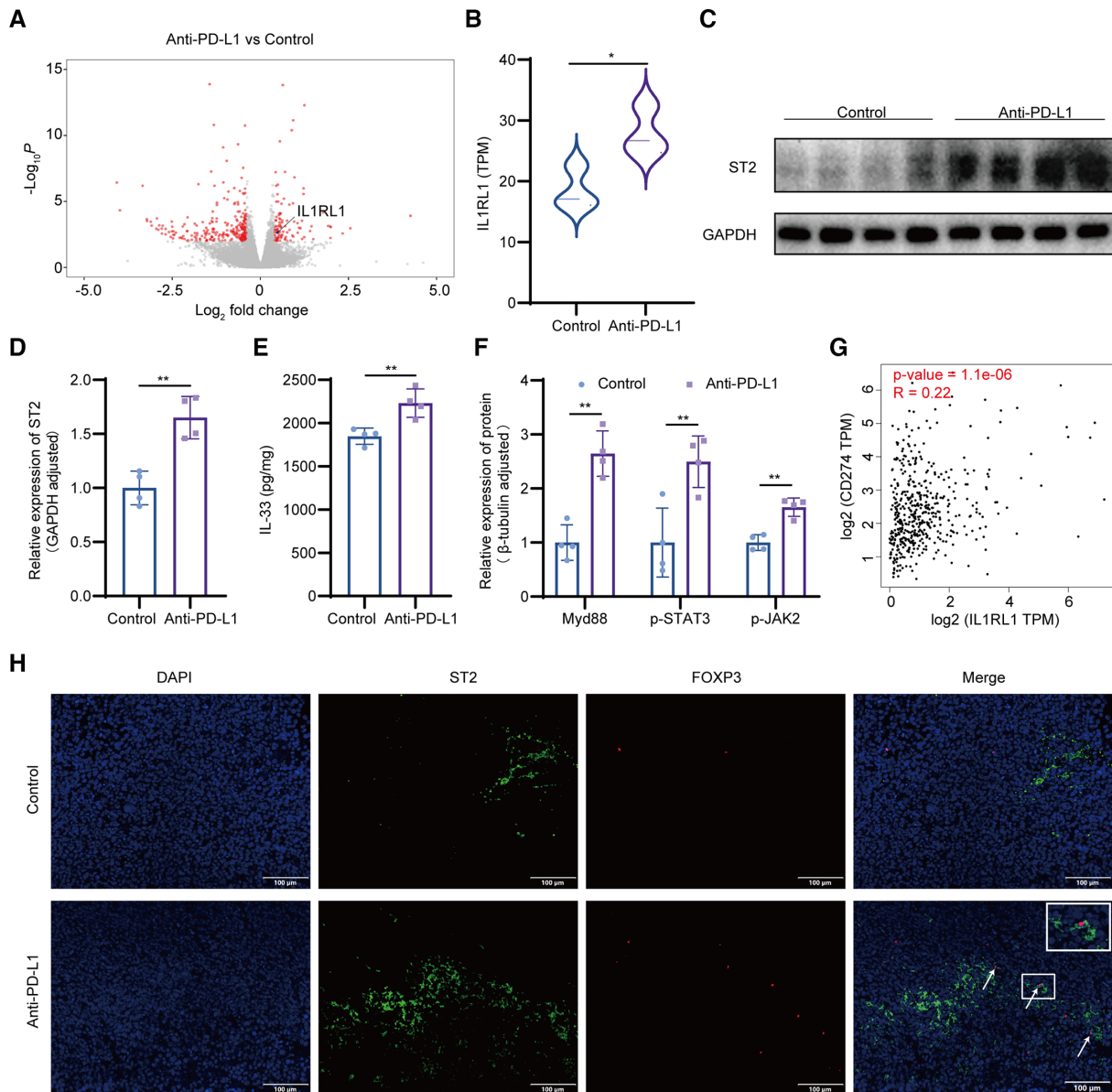


Figure 1 IL-33/ST2 signal upregulated after anti-PD-L1 treatment. Volcano plots generated from analyzing differential gene expression between control and anti-PD-L1 treatment group (A). IL1RL1 gene level in tumor tissues of LLC tumor-bearing mouse injected with anti-PD-L1 (n=3) (B). ST2 protein level in tumor tissues was analyzed by WB (C). The quantification of ST2 expression in tumor tissues during anti-PD-L1 using ImageJ software (n=4) (D). IL-33 tumor tissue expression was analyzed by ELISA (n=4) (E). The expression of Myd88 and activation of JAK2/STAT3 pathway in tumor tissues treated with anti-PD-L1 (F). The gene correlation among CD274 and IL1RL1 in LUAD was analyzed using GEPIA (G). Representative images of ST2 (green) and FOXP3 (red) labeled in the LLC tumor tissues after anti-PD-L1 treatment (H). Scale bar=100 μm. White arrows point to ST2⁺FOXP3⁺ cells. *P < 0.05, **P < 0.01. GEPIA, Gene Expression Profiling Interactive Analysis; LLC, lewis lung carcinoma; LUAD, lung adenocarcinoma.

elevation in ST2 expression within tumor tissues after anti-PD-L1 treatment. A pronounced increase in ST2-positive cells, as highlighted in [figure 1H](#), was particularly evident within Tregs, defined as positive FOXP3 cells. More importantly, in patients with lung and colon cancer, IL-33 and IL1RL1 transcript levels were upregulated in tumor tissues compared with adjacent normal tissues (online supplemental figure 3). In lung cancer tumors during pembrolizumab treatment, expression of IL1RL1 levels was significantly higher in pretreatment tumor tissues and non-responded tumor tissues compared with responded tumor tissues (online supplemental figure 3a). Expression of IL-33 and IL1RL1 levels was significantly decreased in responded tumor tissues than in non-responded tumor tissues in colon cancer patients treated with pembrolizumab (online supplemental figure 3b). Additionally, Gene Expression Profiling Interactive Analysis databases identified a significant positive gene correlation between CD274 and IL1RL1 in lung adenocarcinoma ([figure 1G](#)), underscoring the potential for tumor therapy by targeting IL-33 and PD-L1.

Disruption of the IL-33/ST2 signal enhances the therapeutic effect of anti-PD-L1

To determine the role of IL-33/ST2 axis in atezolizumab treatment, the antitumor effect of sST2-Fc, a fusion protein blocking IL-33/ST2 signal, was assessed and combined with atezolizumab in multiple tumor models. Individually, either atezolizumab or sST2-Fc monotherapy resulted in a partial postponement of tumor growth. However, their combined application led to a substantial enhancement of antitumor efficacy in both subcutaneous CT26 ([figure 2A](#)) and LLC ([figure 2B](#)) models. To confirm the potential of dual targeting IL-33 and PD-L1 in suppressing tumor metastasis and extending survival, metastatic models were established for both CT26 and LLC. In the metastatic CT26 model, the control group exhibited a median survival of 20 days while anti-PD-L1 monotherapy extended the median survival to 39 days. Moreover, a further prolongation of overall survival in mice was observed after treating with anti-PD-L1 and sST2-Fc, with an undetermined median survival time on day 50 (vs the control group) ([figure 2C](#)). In the LLC metastatic model, the results demonstrated that both anti-PD-L1 and sST2-Fc monotherapies effectively reduced lung metastases. However, the combination therapy of atezolizumab and sST2-Fc demonstrated even greater potency, leading to further inhibition of lung metastasis compared with either monotherapy group ([figure 2D](#)). Collectively, these findings suggested that blocking IL-33 could enhance the effectiveness of atezolizumab immunotherapy.

Combinational therapy of sST2-Fc and anti-PD-L1 enhanced the immune response of T cell

To elucidate the underlying mechanism of the combinational injection of sST2-Fc and anti-PD-L1, bulk RNA sequencing (RNA-seq) was performed on LLC tumor tissues subjected to a variety of treatments. As

anticipated, genes associated with cytotoxicity of CD8⁺ T cell, such as *Prfl* (perforin), *Ifng* (interferon- γ) and *Gzmb* (granzyme B), were markedly upregulated in combination-treated samples relative to control or monotherapies ([figure 3A](#)). The impact of the combinational therapy on different facets of the TME, particularly focusing on T-cell dynamics, was further assessed. This assessment included scoring for T cell activity ([figure 3B](#)), IFN- γ response ([figure 3C](#)), and IFN- α response ([figure 3D](#)), all of which were notably higher in the combination therapy compared with monotherapy groups. The GSEA unveiled that, compared with the anti-PD-L1 group, the combined treatment group demonstrated significant enrichment in various biological processes ([figure 3E](#)). Subsequent GO and KEGG enrichment analyses highlighted 10 significant immune-related terms and pathways in the combined therapy group, presented in online supplemental figure 4a,b.

In the subcutaneous CT26 model, using a combined blockade of IL-33 and PD-L1 led to a notable decrease in both the absolute number and the percentage of CD4⁺ T cells in tumor tissues ([figure 3I](#) and online supplemental figure 4c), especially affecting CD4⁺FOXP3⁺ Tregs ([figure 3J](#)). Furthermore, there was an increase in the number and the percentage of CD8⁺ T cells and CD8⁺GranB⁺ cells in tumor tissues of the combined therapy group ([figure 3F,G](#) and online supplemental figure 4d,f). Specifically, the dual blockade therapy resulted in a significantly higher number and percentage of CD8⁺IFN- γ ⁺ cells detected within tumor tissues compared with the control group or monotherapy groups ([figure 3H](#) and online supplemental figure 4e). These findings showed that dual blockade approach induces an enhanced T-cell response, characterized by increased CD8⁺IFN- γ ⁺ cells and CD8⁺GranB⁺ cells, along with a simultaneous decrease in Tregs within tumor tissues.

Generation, characterization and bioactivity of bifunctional fusion proteins targeting both PD-L1 and IL-33

To specifically target IL-33 in the TME, bifunctional anti-PD-L1-sST2 and sST2-anti-PD-L1 fusion proteins were developed, which concurrently targeted PD-L1 and IL-33 via fusing sST2 to the N-terminus or C-terminus of the atezolizumab heavy chain using a flexible (Gly4Ser)₃Gly linker as well as the light chain of atezolizumab unaltered ([figure 4A](#)). Non-reduced and reduced SDS-PAGE results showed that both bifunctional fusion proteins had expected molecular weight and high purity ([figure 4B,C](#)). The binding affinity and kinetic parameters of the bifunctional fusion proteins with human PD-L1 (hPD-L1) ([figure 4D](#)) or mouse IL-33 (mIL-33) ([figure 4E](#)) were detected. The results demonstrated that two forms of bifunctional fusion proteins exhibited comparable affinity to hPD-L1 and mIL-33 as seen with anti-PD-L1 or sST2-Fc. The inhibitory effect of two forms of bifunctional fusion proteins on the PD-L1 pathway in vitro was investigated by the luciferase reporter gene system based

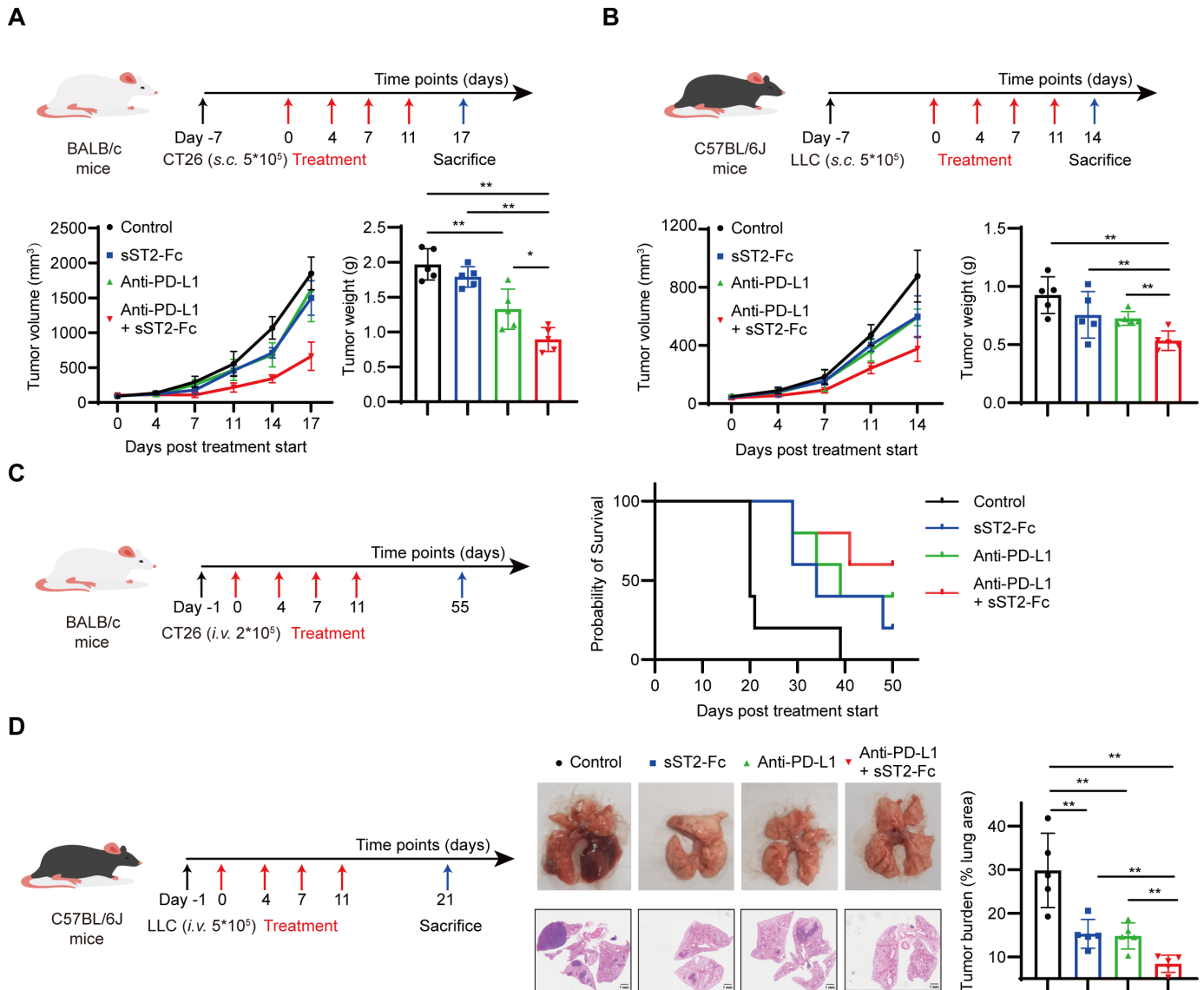


Figure 2 Dual targeting of PD-L1 and IL-33 enhanced antitumor effect of anti-PD-L1 therapy in mouse models. Treatment scheme (top), tumor growth curves (bottom left), and tumor weight (bottom right) of CT26 (A) or LLC (B) tumor-bearing mice in four groups ($n=5$). Schematic diagram of treatment protocol (left) and survival curves (right) of metastasis CT26 tumor model ($n=5$) (C). Scheme (left), H&E-stained lung tissues together with their representative photos (middle), and the quantity of tumor burden (right) from each group with metastasis LLC tumor ($n=5$) (D). * $P < 0.05$, ** $P < 0.01$. LLC, lewis lung carcinoma.

on NAFT activation. This analysis yielded EC₅₀ of 0.5, 0.4, and 1.0 nM for atezolizumab, anti-PD-L1-sST2, and sST2-anti-PD-L1, respectively (figure 4F). Further investigations revealed that IL-33 significantly augmented the percentage of FOXP3⁺ cells differentiated from Naïve CD4⁺ T cells, an effect completely nullified in the presence of sST2-Fc, and two forms of bifunctional fusion proteins (figure 4G). To further determine the bioactivity of the sST2 component in bifunctional fusion proteins, its effect was examined via testing LPS-induced IL-6 and TNF- α cytokines production from RAW264.7 cells in vitro. The results displayed that the levels of IL-6 (figure 4H) and TNF- α (figure 4I) were significantly inhibited by pretreatment with both sST2-Fc and bifunctional fusion proteins. Meanwhile, the safety of two fusion proteins in vivo was confirmed by H&E staining, and the results showed no

morphological damage in major organs of mice injected with anti-PD-L1-sST2 and sST2-anti-PD-L1 (online supplemental figure 5). In conclusion, these data suggested that both bifunctional fusion proteins were successfully constructed and had dual-blocking biological effects on PD-L1 and IL-33.

Simultaneous targeting of PD-L1 and IL-33 induces enhanced antitumor activity

To investigate the biological effect of bifunctional fusion proteins in vivo, the antitumor effect of bifunctional fusion proteins was evaluated in mouse tumor models. Treatment with bifunctional fusion proteins significantly inhibited LLC tumor growth and reduced tumor weight, demonstrating consistency with the effects observed in the combination therapy. Remarkably, anti-PD-L1-sST2

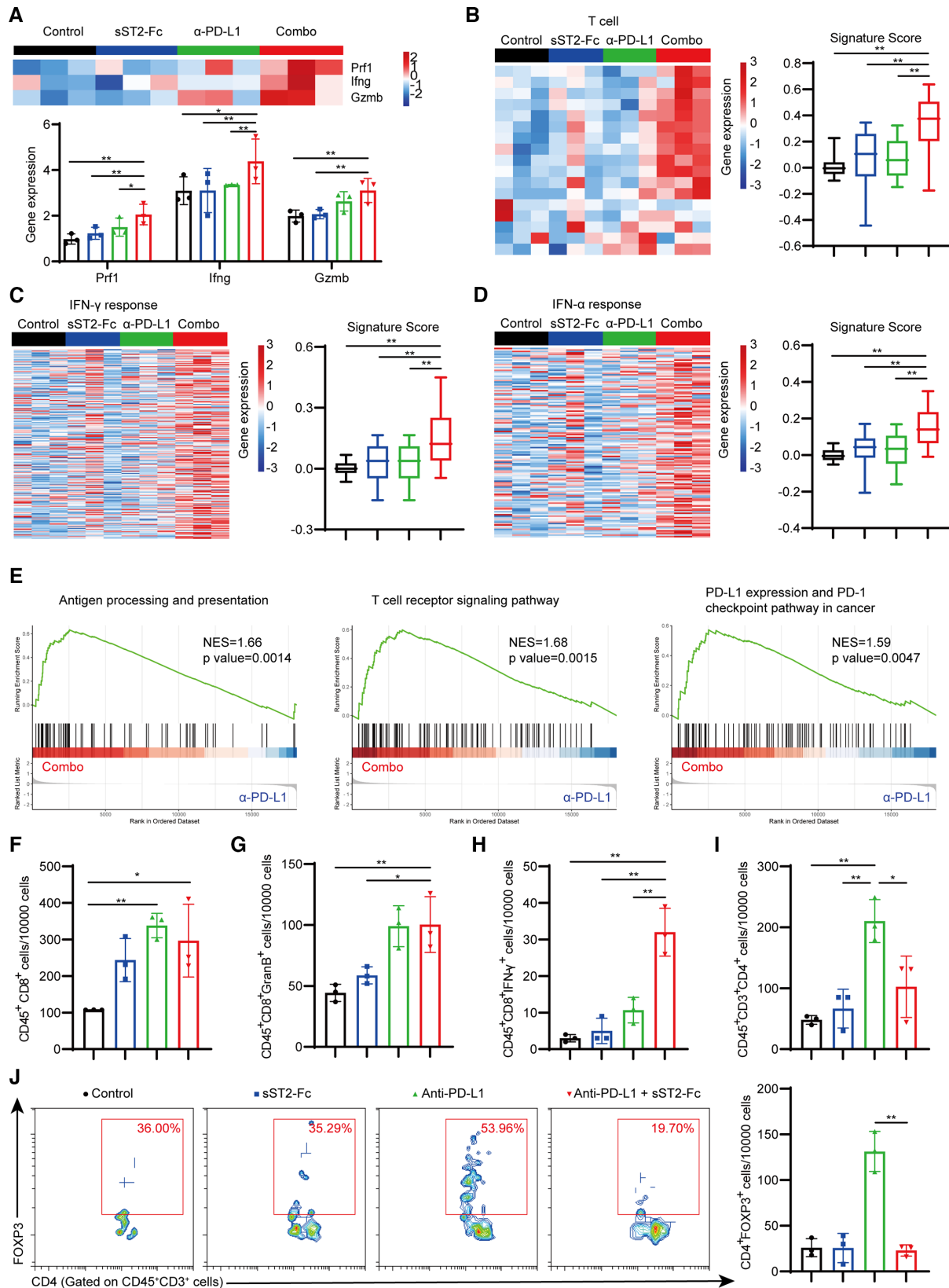


Figure 3 Combined blockade of IL-33 and PD-L1 enhanced T cells response. Bulk RNA-seq to evaluate immune landscape in LLC tumors (A–E). Gene expression levels of *Prf1*, *Ifng*, and *Gzmb* in tumor tissue of LLC tumor-bearing mice (n=3) (A). The data were presented in Log₂TPM and every group was compared with the combination therapy group. Heat map of genes that under the category of immune signatures (n=3) (B–D). Gene set enrichment analysis enrichment plot of KEGG pathway for genes in Combo-treated tumors, relative to anti-PD-L1-treated tumors (E). Flow cytometry was used to analyze the absolute number of CD4⁺ (F), CD8⁺ (G), CD8⁺GranB⁺ (H) and CD8⁺IFN- γ ⁺ (I) cells and CD4⁺FOXP3⁺ cells (J) in CT26 tumor tissues (n=3). *P < 0.05, **P < 0.01. LLC, lewis lung carcinoma.

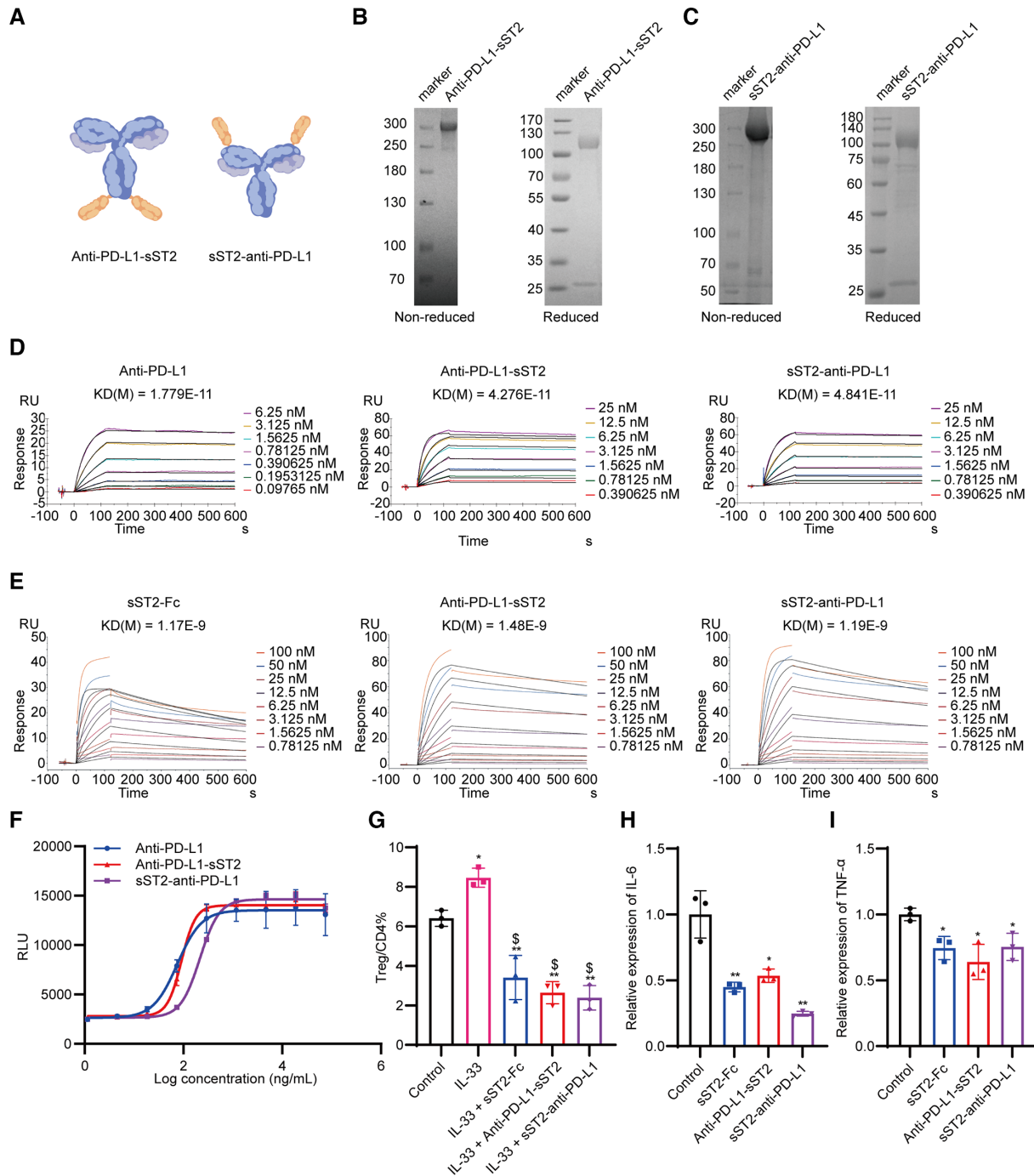


Figure 4 Construction and characterization of bifunctional fusion proteins targeting both PD-L1 and IL-33. Structure of bifunctional fusion proteins (A). Atezolizumab and sST2 were used to targeting PD-L1 and IL-33, respectively, and were fused by a flexible (Gly4Ser)3Gly linker. The purity determination of anti-PD-L1-sST2 (B) and sST2-anti-PD-L1 (C). Affinity of bifunctional fusion proteins for hPD-L1 (D) or mIL-33 (E) proteins measured by SPR. PD-1/PD-L1 blockade bioassay of bifunctional fusion proteins was confirmed (n=2) (F). Naïve CD4⁺ T cells were incubated with anti-CD3/CD28 and TGF-β₁, subjected to the specified treatments for 3 days to determine the frequencies of FOXP3⁺ T cells (n=3) (G). Effects of bifunctional fusion proteins on LPS-induced production of IL-6 (H) and TNF-α (I) from Raw264.7 in vitro (n=3). * and \$ represent the Student's t-test of each groups compared with control group and IL-33 group, respectively. *P < 0.05, **P < 0.01, \$P < 0.05.

treatment resulted in a substantial suppression of tumor progression and a significant diminishment in tumor weight. These effects surpassed those observed in both the sST2-anti-PD-L1 and combination therapy treatment groups, emphasizing that anti-PD-L1-sST2 is a more efficacious format for in vivo study (figure 5A,B). The

antineoplastic activity of anti-PD-L1-sST2 was further tested in an experimental metastasis lung tumor model (figure 5C). Despite all mice treated with monotherapies or combination therapy died within 70 days, a noteworthy 25% of mice treated with anti-PD-L1-sST2 survived until day 100 (figure 5D), suggesting that anti-PD-L1-sST2

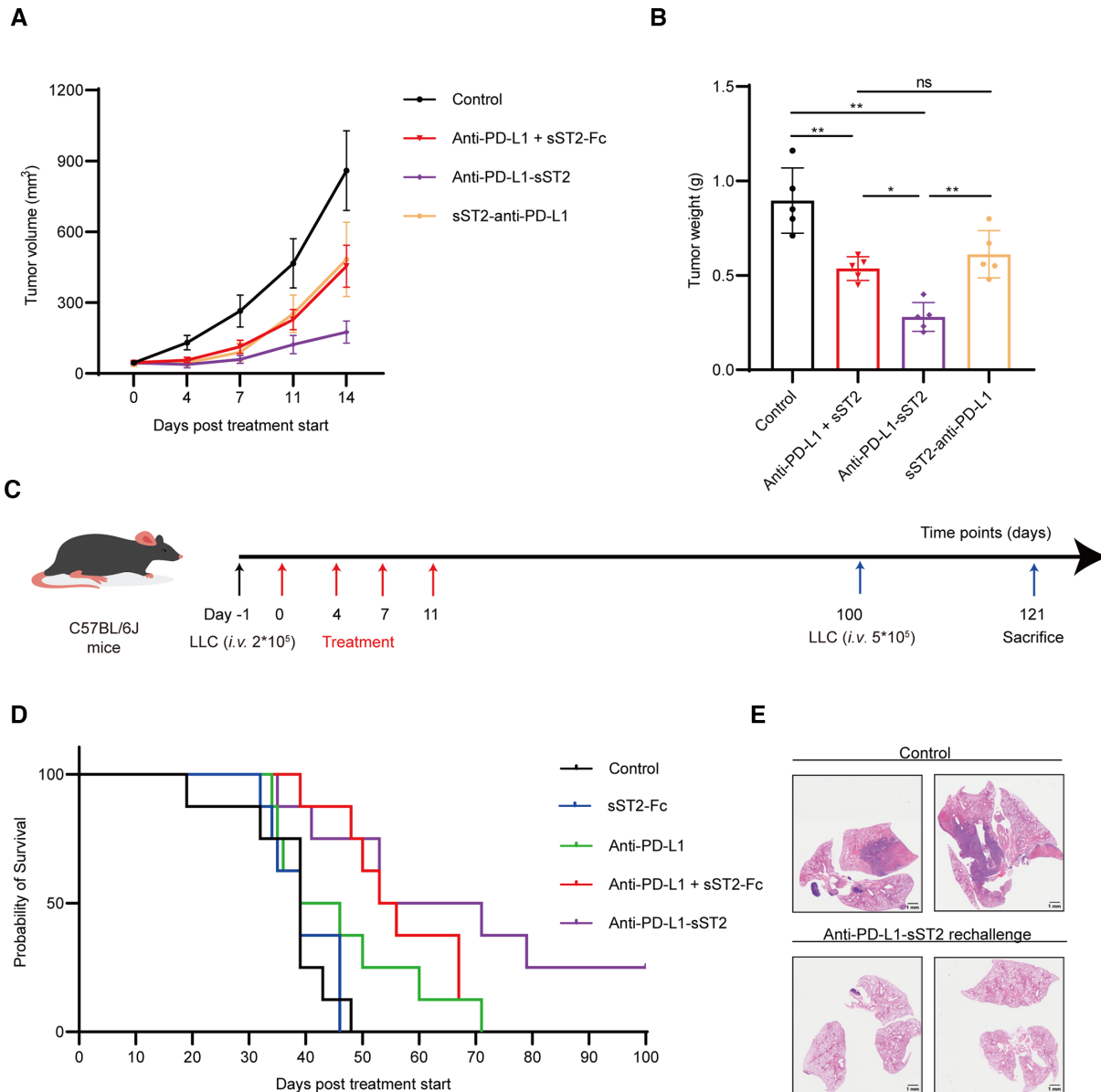


Figure 5 Antitumor activity of bifunctional fusion proteins in murine LLC models. Tumor growth (A) and tumor weight (B) of LLC tumor-bearing mice theraped with bifunctional fusion proteins (11.5 mg/kg) or anti-PD-L1 (7.5 mg/kg) and sST2-Fc (6.3 mg/kg) combined therapy (n=5). Schematic overview of the experimental study (C). Mice were intravenously injected with LLC cells (2×10^5), treated at day 0, 4, 7, and 11 after injection (red arrows) and observed until day 100 (n=8). Then, the survived mice were rechallenged with injection of 5×10^5 LLC cells and observed for three additional weeks. Survival curves of tumor-bearing mice in five groups (D). H&E-stained lung tissues of mice in rechallenge assay (E). * $P < 0.05$, ** $P < 0.01$. LLC, lewis lung carcinoma.

significantly improved the overall survival. Mice that survived in the anti-PD-L1-sST2 group were rechallenged and exhibited a potent activity to prevent metastatic nodules compared with control mice (figure 5E). These data suggested that both bifunctional fusion proteins displayed potent antitumor effects, especially anti-PD-L1-sST2.

Anti-PD-L1-sST2 induced immunoinflammatory TME in the LLC tumor model

To elucidate the possible mechanisms contributing to the potent antitumor activity of anti-PD-L1-sST2, the tumor-infiltrating immune cells repertoire was examined by scRNA-seq (figure 6A). A total of 65,879 cells from tumor

tissues in four groups, control (19,951 cells), anti-PD-L1 (15,215 cells), anti-PD-L1 + sST2Fc (14,863 cells) and anti-PD-L1-sST2 (15,850 cells), were sequenced and subjected to an unsupervised clustering analysis, which identified 10 clusters (figure 6B) according to marker gene expression (online supplemental figure 6a,b). Increased proportion of tumor-infiltrating immune cells, including monocytes, neutrophils, DC, NK and T cells, were observed in groups of atezolizumab, combined therapy and anti-PD-L1-sST2 compared with control group (online supplemental figure 6c). Of interest, scRNA-seq depicted 10 distinct subclusters of 2881T cells based on specific marker gene expression (online supplemental figure 6d,e,h).

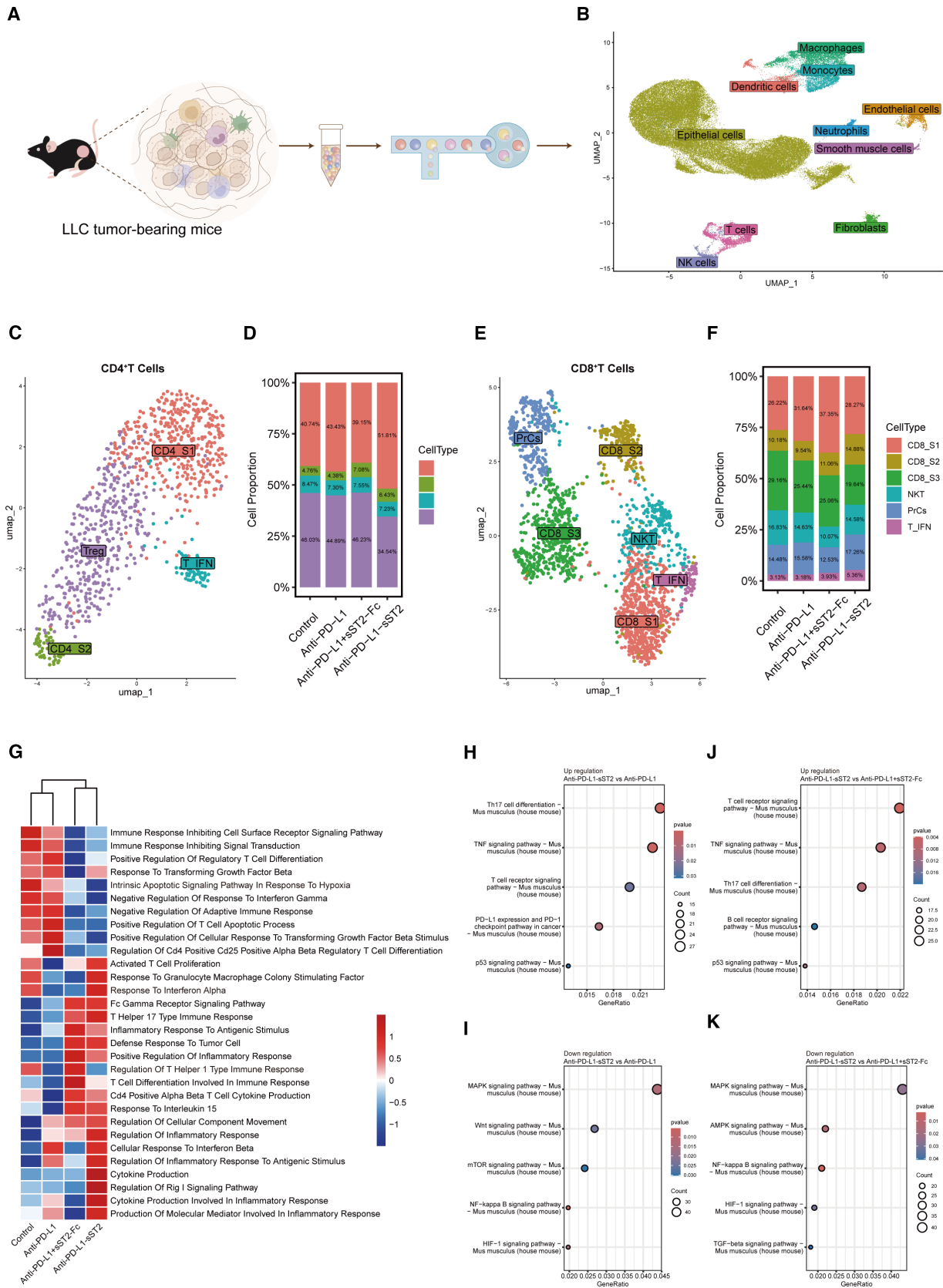


Figure 6 Dual targeting of PD-L1 and IL-33 changed T-cell cellular landscapes. Design of scRNA-seq experiment (A). UMAP of all cell types from four groups (B). UMAP plots showing all CD4⁺ (C) and CD8⁺ (E) T cells from tumor tissues in four groups. Bar plots exhibiting the proportion of CD4⁺ (D) and CD8⁺ (F) T cells within each cluster. Selected significantly enriched pathways in KEGG analyses based on the differentially expressed genes in T cell clusters (G). Gene Ontology in biological function enrichment analysis of the upregulated (H, J) or downregulated (I, K) expressed genes in T cells of anti-PD-L1-sST2 versus atezolizumab group, and anti-PD-L1-sST2 versus combination group, respectively. LLC, lewis lung carcinoma.

Following anti-PD-L1-sST2 treatment, compared with atezolizumab, both the number and fraction of exhausted CD8_S3 cluster T cells decreased while $\gamma\delta$ T cluster T cells increased (online supplemental figure 6f,g). The proportion of effector CD8⁺ T cells within T cells increased after combined therapy compared with atezolizumab monotherapy (online supplemental figure 6g). Further, in-depth scRNA-seq clustering of the CD8⁺ and CD4⁺ T cells population yielded six subclusters and four subclusters, respectively (figure 6C,E). Notably, following anti-PD-L1-sST2 therapy, increased CD4_S1 and decreased Treg and CD8_S3 were detected in TME compared with anti-PD-L1 treatment and combination treatment, as well as an increased effector CD8⁺ T cells compared with atezolizumab (figure 6D,F). DEGs of T cells were used to perform enriched functions analyze of KEGG pathway and Go terms in TME following different treatments. As illustrated in figure 6G, the pathway analysis results revealed significant enrichment of enhanced immune responses, such as T cell proliferation and cytokine production, in T cells of the anti-PD-L1-sST2 or combination group. Comparing versus anti-PD-L1-treated tumors, the anti-PD-L1-sST2 fusion protein illustrated the upregulation of genes associated with the signaling pathway of T cell receptor, TNF, and p53 signaling pathway, as well as the downregulation of genes associated with the signaling pathway of MAPK, Wnt and NF-kappa B (figure 6H,I). Comparing versus combined treated tumors, anti-PD-L1-sST2 fusion protein illustrated upregulation of genes associated with signaling pathway of T cell receptor, TNF, Th17 cell differentiation and p53, as well as downregulation of genes associated with signaling pathway of NF-kappa B, HIF-1 and TGF-beta (figure 6J,K). Collectively, these results indicated that anti-PD-L1-sST2 treatment drove a remodeling of tumor-infiltrating immune cells, thereby triggering immune responses.

The scRNA-seq T-cell immunophenotyping was further validated through cytoflow assay and IF results. As shown in the figure 7, anti-PD-L1-sST2 treatment significantly elevated the infiltration of CD8⁺ T cells (figure 7A), cytotoxic T cells (CD3⁺CD8⁺IFN- γ ⁺) (figure 7B), memory CD8⁺ T cells (CD44⁺CD8⁺) (figure 7C), and stem-like CD8⁺ T cells (CD8⁺TCF-1⁺) (figure 7D) compared with vehicle or monotherapy. Notably, when compared with combination therapy, anti-PD-L1-sST2 treatment remarkably reduced the presence of exhausted CD8⁺ T cells (CD8⁺PD-1⁺TIM-3⁺) within the TME (figure 7E). Meanwhile, anti-PD-L1-sST2 treatment decreased CD4⁺FOXP3⁺ Tregs infiltration compared with atezolizumab monotherapy (figure 7G). Collectively, these findings provide additional evidence that anti-PD-L1-sST2 promoted T-cell responses in TME. Furthermore, an exploration of various components within the TME was undertaken to unravel additional mechanisms. In LLC tumor tissues, on anti-PD-L1-sST2 treatment, there was a noticeable downregulation in the expression of collagen (figure 7F and online supplemental figure 8), α -SMA (figure 7H), vimentin (figure 7I), TGF- β 1 (figure 7J and online supplemental

figure 7), and coupled with an upregulation in E-cadherin protein levels (figure 7K and online supplemental figure 9) compared with the control or monotherapies. In conclusion, these findings suggested that the immunosuppressive TME state in LLC tumor was attenuated after simultaneously targeting PD-L1 and IL-33, especially through anti-PD-L1-sST2 bifunctional fusion protein treatment.

DISCUSSION

Resistance to PD-L1 checkpoint blockade is caused by various factors in the TME, including inadequate infiltration of immune cells, accumulation of immunosuppressive Tregs and factors.^{1,35} This article reports a substantial increase in ST2⁺ Tregs, immunosuppressive cells modulated by IL-33, observed during anti-PD-L1 therapy. This phenomenon raises concerns about the potential undermining of the effectiveness of the treatment. Meanwhile, targeting IL-33 with sST2-Fc effectively inhibited ST2⁺ Tregs, which sequentially enhanced the antitumor activity of anti-PD-L1. To selectively deplete IL-33 in TME, a bispecific fusion protein anti-PD-L1-sST2 was designed and showed an improved therapeutic effect than mono or their combination therapy in local and metastatic LLC models. The impressive antitumor results of anti-PD-L1-sST2 underscore the potential of specifically targeting IL-33 within the TME as an alternative strategy to amplify the tumor-suppressing impact of atezolizumab tumor immunotherapy.

The IL-33/ST2 signal fulfills vital roles in homeostasis and immunity by inducing immune responses of type 2 helper T cells, macrophages, innate lymphoid type 2 cells, and Tregs.^{36–40} Based on the important contribution of IL-33 in allergic inflammation, several biological agents targeting IL-33 are in clinical development (phase 1, 2, or 3) for asthma, chronic obstructive pulmonary disease (COPD), and other allergic diseases. In which, two mAbs against IL-33 (tozorakimab⁴¹ and itepekimab),⁴² and one mAb against ST2 (astegolimab)⁴³ are ongoing phase 3 trials in COPD. ST2 expression in Tregs played a critical role in the expansion and accumulation of Tregs.^{22–44} On allergen exposure, IL-33 signaling on ST2⁺ Tregs was found to suppress the activation and function of $\gamma\delta$ T cells in lung, suppressing the early innate immune response to mucosal injury.³⁸ In tumor progression, ST2⁺ Tregs were found to interact with EGFR-positive CAFs resulting in enhanced immunosuppressive TME and promoting tumor growth.³¹ However, the function of IL-33/ST2 interaction and signaling on ST2⁺ Tregs is unclear in PD-L1 ICIs. In our research, we explored the role of IL-33/ST2 axis during atezolizumab treatment and found significantly increased the IL-33 and ST2L protein expression. Furthermore, a significant increase of ST2-positive Tregs in tumor tissue was observed following PD-L1 treatment, which may be a critical mechanism limiting the antitumor effect of atezolizumab therapy. Building on this investigation, we subsequently showed that sST2-Fc fusion protein

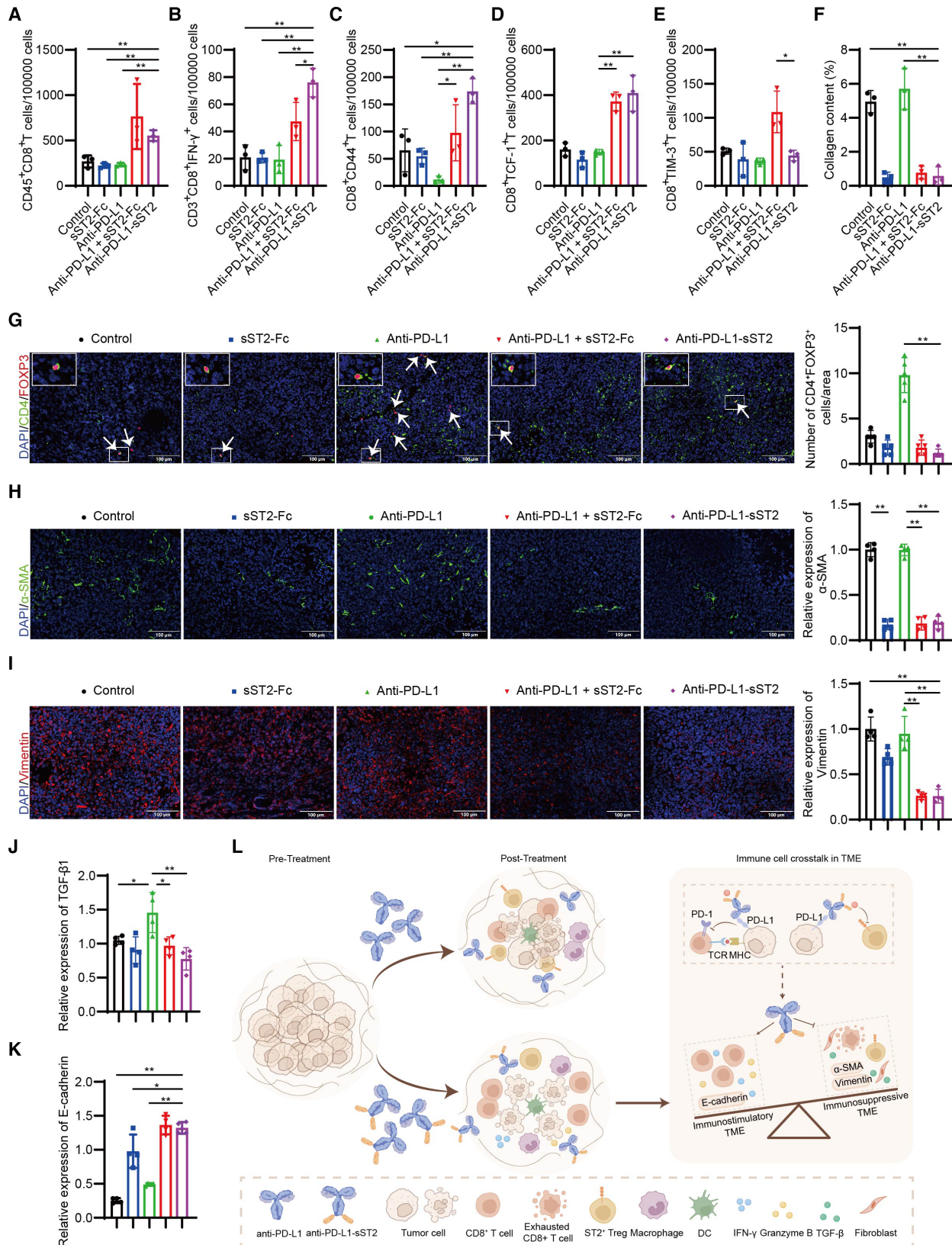


Figure 7 Dual targeting of PD-L1 and IL-33 reprograms immuno-inflammatory phenotype TME. Absolute number of CD8⁺ cells (A), CD3⁺CD8⁺IFN- γ ⁺ T cells (B), CD8⁺CD44⁺ cells (C), CD8⁺TCF-1⁺ cells (D), CD8⁺TIM-3⁺ cells (E) within the CD45⁺ cells from tumor tissues (n=3). The quantification of collagen (n=3) (F). The quantification of CD4⁺FOXP3⁺ cells in LLC tumor-bearing mice (n=5) (G). White arrows point to CD4⁺FOXP3⁺ cells. The quantification of α -SMA (H), Vimentin (I), TGF- β 1 (J), and E-cadherin (K) (n=4). In **figure 7G–K**, data in groups of control, sST2-Fc, anti-PD-L1, anti-PD-L1 + sST2 Fc, and anti-PD-L1-sST2 are shown in color of blank, blue, green, red, and violet, respectively. Schematic diagram illustrating the potent antitumor impact of anti-PD-L1-sST2 bifunctional fusion protein (l). *P < 0.05, **P < 0.01. LLC, lewis lung carcinoma; TME, tumor microenvironment.

treatment, blocking the activation signal of IL-33 on ST2⁺ Tregs, notably enhanced antitumor activity of atezolizumab treatment in both subcutaneous and metastatic tumor models. Indeed, scRNA-seq and flow cytometry analyses of tumor tissues showed that dual targeting of IL-33 and PD-L1 exerted superior antitumor effects by enhancing T-cell responses; it reduced tumor-infiltrating Tregs and exhausted CD8⁺ T cells while increasing tumor-infiltrating cytotoxic T lymphocyte cells (CTLs), stem-like CD8⁺ T cells, and memory CD8⁺ T cells and $\gamma\delta$ T cells. The underlying mechanism of antitumor activity was also reflected in the effects on other components of TME: reduced expression of α -SMA, TGF- β , vimentin and collagen, and increased E-cadherin protein level.

Several preclinical studies have discussed the correlation between IL-33/ST2 signal and the antitumor effect of PD-1/PD-L1 ICIs in different tumor models.^{45–49} In pancreatic ductal adenocarcinomas and MC38 tumor models, IL-33 was found to upregulate the PD-1 levels in tumor group 2 innate lymphoid cells (ILC2s) and interact with ST2 expressed in CD8⁺ T cells, sensitizing tumors to the anti-PD-1 therapy.^{45,46} However, those antitumor activities induced by IL-33, such as accumulation and effector function of CD8⁺ T cells, were limited by IL1RL1⁺ Treg cells expansion,^{31,50} suggesting a critical targeting role of IL1RL1⁺ Treg cells in enhancing antitumor effect of anti-PD-1/PD-L1 therapy. In our study, we revealed an increased infiltration of IL1RL1⁺ Treg cells in tumor tissues treated with anti-PD-L1, and blocked IL-33/ST2 signal with sST2-Fc fusion protein notably enhanced antitumor activity of anti-PD-L1 treatment. Similarly, in oral squamous cell carcinoma model, IL-33/ST2 was highly expressed in tumor tissues and could promote direct-induced and IFN- γ -induced PD-L1 expression through the activation of JAK2/STAT3 and MyD88/NF- κ B pathway, respectively.⁴⁸ In 4T1 and CT26 subcutaneous tumor models, anti-IL33 injection or ST2^{-/-} mice were combined with anti-PD-1 treatment to facilitate tumor regression by inducing NK cell antitumor responses.⁴⁹ Consistent with these studies, we found that dual targeting of IL-33 and PD-L1, especially using a bifunctional fusion protein anti-PD-L1-sST2, induced potent antitumor responses and notably enhanced antitumor activity.

The concept of bifunctional fusion proteins is to simultaneously target two molecules using one protein. Most of the bifunctional fusion proteins focus on delivering immunostimulatory cytokines to TME, such as IL-15,⁵¹ IL-21⁵² and IL-2,⁵³ leading to superior antitumor effects with lower side effects. These bifunctional fusion proteins could enhance the retention of cytokines within tumor tissue while the accessibility of effector T cells to these immunostimulatory cytokines in the TME may remain constrained, especially in TME with low immune cell infiltration. In contrast, other types of bifunctional fusion proteins aim to modulate the immunosuppressive TME, such as those targeting TGF- β signaling in TME with anti-PD-L1 antibody, including M7824¹³ and BR102,¹² all of which led to significant tumor control. However,

these bifunctional fusion proteins showed modest antitumor activity in tumor models with poorly immunogenic TME.¹⁷ Based on the immunosuppressive function of ST2⁺ Tregs in TME, we hypothesized that the bifunctional fusion proteins dual targeting PD-L1 and IL-33 may facilitate specific targeting of IL-33 signaling in TME compared with non-targeting sST2-Fc, thereby remodeling the TME and inhibiting tumor progression. In the present investigation, two bispecific fusion proteins, anti-PD-L1-sST2 and sST2-anti-PD-L1, were constructed to simultaneously target PD-L1 and IL-33. Notably, the therapeutic effect of anti-PD-L1-sST2 is even superior to combined therapy and sST2-anti-PD-L1. Moreover, anti-PD-L1-sST2 significantly prolonged the survival of 25% mice to 100 days and remained further antimetastatic effect in LLC metastatic model, indicating the potential of targeting IL-33 and PD-L1 for tumor therapy. Bifunctional proteins with different structures differ in some aspects of in vitro or in vivo activity.^{54,55} In a cell-based reporter gene assay (figure 4F), anti-PD-L1-sST2 showed more potent PD-L1-blocked biological activity compared with sST2-anti-PD-L1, as evidenced by the EC50 of anti-PD-L1-sST2 (EC50=0.4nM) being half that of sST2-anti-PD-L1 (EC50=1nM), which may partially explain why anti-PD-L1-sST2 has superior antitumor efficacy to sST2-anti-PD-L1 in vivo. Meanwhile, better PD-1/PD-L1 blocking activity may mean better tumor targeting effects mediated by PD-L1 targeting, leading to improved tumor control. We speculated that some potential factors might also account for the antitumor effect in vivo, such as drug's kinetics in vivo, bioactivity stability, and conformational space, which need further exploration in the design and druggability assessment of protein molecules. Our study highlights the importance of choosing the appropriate format for constructing bispecific fusion proteins to achieve potent antitumor effect.

In conclusion, our results exhibited that ST2⁺ Tregs infiltration was highly increased in TME during anti-PD-L1 therapy and sST2-Fc enhanced antitumor effect of PD-L1-blocked therapy via upregulating the T cell response signatures and the infiltration of CD8⁺ T cells in tumors. Furthermore, in both local and metastatic LLC models, anti-PD-L1-sST2, a bifunctional fusion protein co-targeting IL-33 and PD-L1, demonstrated promising antitumor effects and remodeled the TME, such as reduced Tregs accumulation, exhausted CD8⁺ T cells infiltration, TGF- β expression, Vimentin protein level, as well as increased levels of tumor-infiltrating CTLs and E-cadherin protein level (figure 7L). Taken together, these findings indicate that by blocking both IL-33 and PD-L1 in the TME not only augmented the T-cell responses but also modulated the TME toward an immuno-inflammatory phenotype. Our results provided novel insights into the immunosuppressive mechanisms of PD-L1 blockade therapy, suggesting that dual targeting IL-33 and PD-L1 therapeutic approaches hold promising potential in further clinical application.

Author affiliations

¹Department of Biological Medicines & Shanghai Engineering Research Center of Immunotherapeutics, Fudan University School of Pharmacy, Shanghai, China

²College of Literature, Science, and the Arts, University of Michigan, Ann Arbor, Michigan, USA

³Department of pharmacy, Shanghai Children's Hospital, School of medicine, Shanghai Jiao Tong University, Shanghai, China

Correction notice This article has been corrected since it was first published online. The affiliations have been updated to the following: (1) Fudan University School of Pharmacy, Shanghai, China has been updated to Department of Biological Medicines & Shanghai Engineering Research Center of Immunotherapeutics, Fudan University School of Pharmacy, Shanghai, China(2) University of Michigan, Ann Arbor, Michigan, USA has been updated to College of Literature, Science, and the Arts, University of Michigan, Ann Arbor, Michigan, USA(3) Shanghai Jiao Tong University, Shanghai, China has been updated to Department of pharmacy, Shanghai Children's Hospital, School of medicine, Shanghai Jiao Tong University, Shanghai, China.

Contributors DJ, XW and XuyaoZ designed the study, YN, YB, XH, TW, AZ, ML, ZC and JL performed the experiments; YN, YB, XH, KZ, TW, AZ and ZD analyzed the data; YN, YB, KZ and ZD made the figures; YN, YB, AZ, XumengZ, XZ and JF drafted and revised the paper. All authors approved the final version of this manuscript. DJ, XW and XuyaoZ responsible for the overall content as the guarantor.

Funding This work was supported by grants from National Key Research and Development Program of China (2023YFC3404000, 2023YFC3606600 and 2023YFC3503400), the National Natural Science Foundation of China (82371781, 82073752 and 32200745), and Shanghai Sailing Program (21YF1401900).

Competing interests None declared.

Patient consent for publication Not applicable.

Ethics approval Procedures involving mice were performed in accordance with the standards of Fudan University and approved by Animal Ethical Committee of School of Pharmacy Fudan University (ethical permit 2020-12-SY-ZXY-01).

Provenance and peer review Not commissioned; externally peer reviewed.

Data availability statement Data are available on reasonable request. The datasets used and/or analyzed during this study are available from the corresponding author on reasonable request.

Supplemental material This content has been supplied by the author(s). It has not been vetted by BMJ Publishing Group Limited (BMJ) and may not have been peer-reviewed. Any opinions or recommendations discussed are solely those of the author(s) and are not endorsed by BMJ. BMJ disclaims all liability and responsibility arising from any reliance placed on the content. Where the content includes any translated material, BMJ does not warrant the accuracy and reliability of the translations (including but not limited to local regulations, clinical guidelines, terminology, drug names and drug dosages), and is not responsible for any errors and/or omissions arising from translation and adaptation or otherwise.

Open access This is an open access article distributed in accordance with the Creative Commons Attribution Non Commercial (CC BY-NC 4.0) license, which permits others to distribute, remix, adapt, build upon this work non-commercially, and license their derivative works on different terms, provided the original work is properly cited, appropriate credit is given, any changes made indicated, and the use is non-commercial. See <http://creativecommons.org/licenses/by-nc/4.0/>.

ORCID iDs

Xuyao Zhang <http://orcid.org/0000-0003-1654-5550>

Dianwen Ju <http://orcid.org/0000-0002-4305-9622>

REFERENCES

- van Gulijk M, van Krimpen A, Schetters S, *et al*. PD-L1 checkpoint blockade promotes regulatory T cell activity that underlies therapy resistance. *Sci Immunol* 2023;8:eabn6173.
- Wang R, Liu H, He P, *et al*. Inhibition of PCSK9 enhances the antitumor effect of PD-1 inhibitor in colorectal cancer by promoting the infiltration of CD8⁺ T cells and the exclusion of Treg cells. *Front Immunol* 2022;13:947756.
- Wang Y, Zhang X, Xu C, *et al*. Targeting 4-1BB and PD-L1 induces potent and durable antitumor immunity in B-cell lymphoma. *Front Immunol* 2022;13:1004475.
- Abril-Rodriguez G, Torrejon DY, Liu W, *et al*. PAK4 inhibition improves PD-1 blockade immunotherapy. *Nat Cancer* 2020;1:46–58.
- Vesely MD, Zhang T, Chen L. Resistance Mechanisms to Anti-PD Cancer Immunotherapy. *Annu Rev Immunol* 2022;40:45–74.
- Tauriello DVF, Sancho E, Battle E. Overcoming TGFβ-mediated immune evasion in cancer. *Nat Rev Cancer* 2022;22:25–44.
- Arce Vargas F, Furness AJS, Solomon I, *et al*. Fc-Optimized Anti-CD25 Depletes Tumor-Infiltrating Regulatory T Cells and Synergizes with PD-1 Blockade to Eradicate Established Tumors. *Immunity* 2017;46:577–86.
- Yi M, Zheng X, Niu M, *et al*. Combination strategies with PD-1/PD-L1 blockade: current advances and future directions. *Mol Cancer* 2022;21:28.
- Marabelle A, Kohrt H, Sagiv-Barfi I, *et al*. Depleting tumor-specific Tregs at a single site eradicates disseminated tumors. *J Clin Invest* 2013;123:2447–63.
- Yi M, Wu Y, Niu M, *et al*. Anti-TGF-β/PD-L1 bispecific antibody promotes T cell infiltration and exhibits enhanced antitumor activity in triple-negative breast cancer. *J Immunother Cancer* 2022;10:e005543.
- Yi M, Zhang J, Li A, *et al*. The construction, expression, and enhanced anti-tumor activity of YM101: a bispecific antibody simultaneously targeting TGF-β and PD-L1. *J Hematol Oncol* 2021;14:27.
- Wu Z-H, Li N, Gao Z-Z, *et al*. Development of the Novel Bifunctional Fusion Protein BR102 That Simultaneously Targets PD-L1 and TGF-β for Anticancer Immunotherapy. *Cancers (Base)* 2022;14:4964.
- Lan Y, Zhang D, Xu C, *et al*. Enhanced preclinical antitumor activity of M7824, a bifunctional fusion protein simultaneously targeting PD-L1 and TGF-β. *Sci Transl Med* 2018;10:eaan5488.
- Paz-Ares L, Kim TM, Vicente D, *et al*. Bintrafusp Alfa, a Bifunctional Fusion Protein Targeting TGF-β and PD-L1, in Second-Line Treatment of Patients With NSCLC: Results From an Expansion Cohort of a Phase 1 Trial. *J Thorac Oncol* 2020;15:1210–22.
- Dodagatta-Marri E, Meyer DS, Reeves MQ, *et al*. α-PD-1 therapy elevates Treg/Th balance and increases tumor cell pSmad3 that are both targeted by α-TGFβ antibodies to promote durable rejection and immunity in squamous cell carcinomas. *J Immunother Cancer* 2019;7:62.
- Ravi R, Noonan KA, Pham V, *et al*. Bifunctional immune checkpoint-targeted antibody-ligand traps that simultaneously disable TGFβ enhance the efficacy of cancer immunotherapy. *Nat Commun* 2018;9:741.
- Yi M, Niu M, Zhang J, *et al*. Combine and conquer: manganese synergizing anti-TGF-β/PD-L1 bispecific antibody YM101 to overcome immunotherapy resistance in non-inflamed cancers. *J Hematol Oncol* 2021;14:146.
- Holgado A, Braun H, Van Nuffel E, *et al*. IL-33trap is a novel IL-33-neutralizing biologic that inhibits allergic airway inflammation. *J Allergy Clin Immunol* 2019;144:204–15.
- Moussion C, Ortega N, Girard JP. The IL-1-like cytokine IL-33 is constitutively expressed in the nucleus of endothelial cells and epithelial cells in vivo: a novel “alarmin”? *PLoS ONE* 2008;3:e3331.
- Wood IS, Wang B, Trayhurn P. IL-33, a recently identified interleukin-1 gene family member, is expressed in human adipocytes. *Biochem Biophys Res Commun* 2009;384:105–9.
- Shen JX, Liu J, Zhang GJ. Interleukin-33 in Malignancies: Friends or Foes? *Front Immunol* 2018;9:3051.
- Li A, Herbst RH, Canner D, *et al*. IL-33 Signaling Alters Regulatory T Cell Diversity in Support of Tumor Development. *Cell Rep* 2019;29:2998–3008.
- Jiang W, Lian J, Yue Y, *et al*. IL-33/ST2 as a potential target for tumor immunotherapy. *Eur J Immunol* 2021;51:1943–55.
- Van der Jeught K, Sun Y, Fang Y, *et al*. ST2 as checkpoint target for colorectal cancer immunotherapy. *JCI Insight* 2020;5:e136073.
- O'Donnell C, Mahmoud A, Keane J, *et al*. An antitumorigenic role for the IL-33 receptor, ST2L, in colon cancer. *Br J Cancer* 2016;114:37–43.
- Luo P, Deng S, Ye H, *et al*. The IL-33/ST2 pathway suppresses murine colon cancer growth and metastasis by upregulating CD40 L signaling. *Biomed Pharmacother* 2020;127:110232.
- Zhou Y, Ji Y, Wang H, *et al*. IL-33 Promotes the Development of Colorectal Cancer Through Inducing Tumor-Infiltrating ST2L⁺ Regulatory T Cells in Mice. *Technol Cancer Res Treat* 2018;17:1533033818780091.
- Sun R, Gao DS, Shoush J, *et al*. The IL-1 family in tumorigenesis and antitumor immunity. *Semin Cancer Biol* 2022;86:280–95.
- Wen Y-H, Lin H-Q, Li H, *et al*. Stromal interleukin-33 promotes regulatory T cell-mediated immunosuppression in head and neck squamous cell carcinoma and correlates with poor prognosis. *Cancer Immunol Immunother* 2019;68:221–32.

- 30 Son J, Cho J-W, Park HJ, *et al.* Tumor-Infiltrating Regulatory T-cell Accumulation in the Tumor Microenvironment Is Mediated by IL33/ST2 Signaling. *Cancer Immunol Res* 2020;8:1393–406.
- 31 Sun R, Zhao H, Gao DS, *et al.* Amphiregulin couples IL1RL1⁺ regulatory T cells and cancer-associated fibroblasts to impede antitumor immunity. *Sci Adv* 2023;9:eadd7399.
- 32 Taniguchi S, Elhance A, Van Duzer A, *et al.* Tumor-initiating cells establish an IL-33-TGF- β niche signaling loop to promote cancer progression. *Science* 2020;369:eaay1813.
- 33 Nan Y, Zhang X, Wang S, *et al.* Targeting CD47 Enhanced the Antitumor Immunity of PD-L1 Blockade in B-Cell Lymphoma. *Immunother (Los Angel)* 2023;15:175–87.
- 34 Van Damme H, Dombrecht B, Kiss M, *et al.* Therapeutic depletion of CCR8⁺ tumor-infiltrating regulatory T cells elicits antitumor immunity and synergizes with anti-PD-1 therapy. *J Immunother Cancer* 2021;9:e001749.
- 35 Yuan Y, Adam A, Zhao C, *et al.* Recent Advancements in the Mechanisms Underlying Resistance to PD-1/PD-L1 Blockade Immunotherapy. *Cancers (Basel)* 2021;13:663.
- 36 Dwyer GK, D'Cruz LM, Turnquist HR. Emerging Functions of IL-33 in Homeostasis and Immunity. *Annu Rev Immunol* 2022;40:15–43.
- 37 Hatzioannou A, Banos A, Sakelaropoulos T, *et al.* An intrinsic role of IL-33 in Treg cell-mediated tumor immunoevasion. *Nat Immunol* 2020;21:75–85.
- 38 Faustino LD, Griffith JW, Rahimi RA, *et al.* Interleukin-33 activates regulatory T cells to suppress innate $\gamma\delta$ T cell responses in the lung. *Nat Immunol* 2020;21:1371–83.
- 39 He D, Xu H, Zhang H, *et al.* Disruption of the IL-33-ST2-AKT signaling axis impairs neurodevelopment by inhibiting microglial metabolic adaptation and phagocytic function. *Immunity* 2022;55:159–73.
- 40 Gordon ED, Simpson LJ, Rios CL, *et al.* Alternative splicing of interleukin-33 and type 2 inflammation in asthma. *Proc Natl Acad Sci U S A* 2016;113:8765–70.
- 41 England E, Rees DG, Scott IC, *et al.* Tozorakimab (MEDI3506): an anti-IL-33 antibody that inhibits IL-33 signalling via ST2 and RAGE/EGFR to reduce inflammation and epithelial dysfunction. *Sci Rep* 2023;13:9825.
- 42 Rabe KF, Celli BR, Wechsler ME, *et al.* Safety and efficacy of itepekimab in patients with moderate-to-severe COPD: a genetic association study and randomised, double-blind, phase 2a trial. *Lancet Respir Med* 2021;9:1288–98.
- 43 Yousuf AJ, Mohammed S, Carr L, *et al.* Astegolimab, an anti-ST2, in chronic obstructive pulmonary disease (COPD-ST2OP): a phase 2a, placebo-controlled trial. *Lancet Respir Med* 2022;10:469–77.
- 44 Kim B-S, Clinton J, Wang Q, *et al.* Targeting ST2 expressing activated regulatory T cells in Kras-mutant lung cancer. *Oncimmunology* 2020;9:1682380.
- 45 Chen L, Sun R, Xu J, *et al.* Tumor-Derived IL33 Promotes Tissue-Resident CD8⁺ T Cells and Is Required for Checkpoint Blockade Tumor Immunotherapy. *Cancer Immunol Res* 2020;8:1381–92.
- 46 Jacquelot N, Seillet C, Wang M, *et al.* Blockade of the co-inhibitory molecule PD-1 unleashes ILC2-dependent antitumor immunity in melanoma. *Nat Immunol* 2021;22:851–64.
- 47 Moral JA, Leung J, Rojas LA, *et al.* ILC2s amplify PD-1 blockade by activating tissue-specific cancer immunity. *Nat New Biol* 2020;579:130–5.
- 48 Zhao M, He Y, Zhu N, *et al.* IL-33/ST2 signaling promotes constitutive and inductive PD-L1 expression and immune escape in oral squamous cell carcinoma. *Br J Cancer* 2023;128:833–43.
- 49 Jovanovic MZ, Geller DA, Gajovic NM, *et al.* Dual blockage of PD-L/PD-1 and IL33/ST2 axes slows tumor growth and improves antitumor immunity by boosting NK cells. *Life Sci* 2022;289:120214.
- 50 Yamagishi R, Kamachi F, Nakamura M, *et al.* Gasdermin D-mediated release of IL-33 from senescent hepatic stellate cells promotes obesity-associated hepatocellular carcinoma. *Sci Immunol* 2022;7:eabl7209.
- 51 Guo J, Liang Y, Xue D, *et al.* Tumor-conditional IL-15 pro-cytokine reactivates anti-tumor immunity with limited toxicity. *Cell Res* 2021;31:1190–8.
- 52 Li Y, Cong Y, Jia M, *et al.* Targeting IL-21 to tumor-reactive T cells enhances memory T cell responses and anti-PD-1 antibody therapy. *Nat Commun* 2021;12:951.
- 53 Ren Z, Zhang A, Sun Z, *et al.* Selective delivery of low-affinity IL-2 to PD-1⁺ T cells rejuvenates antitumor immunity with reduced toxicity. *J Clin Invest* 2022;132:e153604.
- 54 Liang Y, Tang H, Guo J, *et al.* Targeting IFN α to tumor by anti-PD-L1 creates feedforward antitumor responses to overcome checkpoint blockade resistance. *Nat Commun* 2018;9:4586.
- 55 Jin S, Sun Y, Liang X, *et al.* Emerging new therapeutic antibody derivatives for cancer treatment. *Signal Transduct Target Ther* 2022;7:39.